AIAA JOURNAL
Vol. 42, No. 11, November 2004

Sound Produced by Vortex Pairing: Prediction Based on Particle Image Velocimetry

C. Schram*
von Kármán Institute for Fluid Dynamics, 1640 Rhode-St-Genèse, Belgium
A. Hirschberg†
Eindhoven University of Technology, 5600 MB Eindhoven, The Netherlands
and
R. Verzicco‡
Politecnico di Bari, 70125 Bari, Italy

In some cases, the prediction of the sound generated by flows is impaired by inaccuracies in the available flow data. These inaccuracies can be due to the degree of approximation of a flow model, or to the uncertainty of a measurement technique. A particular crucial point for sound prediction is the conservation of the flow invariants. The sound radiated by vortex pairing in a subsonic excited jet is deduced from experimental data obtained by particle image velocimetry. The performance is compared of different formulations of vortex sound theory to predict the corresponding sound production. It is shown that assuming several times the conservation of the momentum and kinetic energy in the implementation of the vortex sound theory improves considerably the robustness of the prediction. In fact, a prediction in good agreement with both a theoretical model of leapfrogging and numerical simulations of merging is obtained, although the basic data do not respect precisely these conservation laws.

Nomenclature

a_e	=	nondimensional velocity perturbation
c_0	=	speed of sound in reference medium
D	=	nozzle outlet diameter
$\boldsymbol{e}$	=	unit vector tangent to ring
f_e	=	acoustical excitation frequency
f_P	=	particle image velocimetry acquisition frequency
$\boldsymbol{I}$	=	identity tensor
$\boldsymbol{n}$	=	unit vector normal to ring plane
P	=	impulse
p'	=	acoustical pressure perturbation
Q	=	Möhring's[11] term (10)
q_M	=	Möhring's[11] acoustical source term (6)
q_P	=	Powell's[12] acoustical source term (5)
r	=	radial coordinate
Sr	=	Strouhal number
T	=	kinetic energy
t	=	time
U_0	=	nozzle outlet velocity
u, v, w	=	velocity components
u'_e	=	velocity perturbation amplitude
$\boldsymbol{v}$	=	velocity vector
$\boldsymbol{x}, \boldsymbol{y}$	=	coordinate
z	=	axial coordinate
z_0	=	vortex centroid axial coordinate (18)
Γ	=	circulation
Γ_{th}	=	theoretical circulation from slug model
Δt_s	=	stroboscopic time increment
θ	=	polar angle
ρ_0	=	fluid density of reference medium
φ	=	phase with respect to the excitation period
$\boldsymbol{\omega}$	=	vorticity vector

Received 19 June 2002; revision received 10 June 2003; accepted for publication 11 July 2003.

*Ph.D. Student, Environmental and Applied Fluid Dynamics Department; currently Research and Development Engineer, Computer-Aided Engineering Division, LMS International, Interleuvenlaan 68, Researchpark Haasrode Z1, B-3001 Leuven, Belgium.

†Professor, Gas Dynamics Group, Fluid Dynamics Laboratory, P.O. Box 513.

‡Associate Professor, Dipartimento di Innovazione Meccanica e Gestionale and Centro di Eccelenza in Meccanica Computazionale, Via Re David 200.

Introduction

THE role played by large-scale coherent structures in the generation of aerodynamic sound by turbulence has been underlined since the very beginning of aeroacoustics. In a review paper, Ffowcs Williams[1] iterates that aeroacoustic analogies at some stage of their derivation always involve the assumption that the turbulent flow possesses some local correlation over a scale l that can be regarded as a typical turbulent eddy size. The size of this eddy is assumed to be small compared to the wavelength of the sound it produces, which defines the concept of compact source. Meanwhile, the analogy[2,3] shows that the acoustical power produced by turbulence is proportional to a local average eddy volume defined on the basis of the scale l.

When subsonic jet noise is considered, three main sources of sound production are investigated: the self-oscillations of vortex rings,[4] the pairing of vortex rings,[5,6] and the breakdown of the rings near the end of the jet potential core.[7] Much effort has been dedicated to the pairing phenomenon, which is also the subject of the present study. Most of the previous investigations (see references cited later) have been based on a theoretical or numerical description of the flow combined with the use of vortex sound theory to predict the corresponding sound production. To the authors' knowledge, the sound emitted by vortex pairing has not yet been predicted on the basis of a purely experimental description of the flowfield. Ryu and Lee[8] stressed the need for a detailed description of the vortex motion that is imposed by the successive time derivatives involved in the aeroacoustical analogy. Bridges and Hussain[7,9] identified the fundamental reason why the use of experimental data to calculate directly the sound production is problematic: the nonconservation of integrals of motion that is due to experimental errors.

This will indeed appear to be a key issue in our work, which involves a measurement of the flowfield. Such a velocity field incorporates some experimental random errors (noise). The work that

is described here makes use of a conservative formulation of vortex sound theory, which appeared previously,[10] to reduce the effect of these random errors. It will be shown that the use of this particular formulation with experimental data provides significantly more robust results than using the original formulations of vortex sound theory.[11,12] In particular, it will be shown that a good agreement is obtained between the sound predicted from the experimental data and both a theoretical model of leapfrogging proposed by Kambe and Minota[13] and Navier–Stokes numerical simulations of vortex merging.[14]

Vortex Sound Analogy

The vortex sound theory has been proposed by Powell[12] as another formulation of Lighthill's[2] aeroacoustical analogy that emphasizes the role played by vorticity in the production of aerodynamic sound. In absence of external forces and neglecting viscothermal effects at low Mach numbers, Powell's analogy[12] yields

$$\frac{1}{c_0^2}\frac{\partial^2 p'}{\partial t^2} - \frac{\partial^2 p'}{\partial x_i^2} = \frac{\partial}{\partial x_i}[\rho_0(\boldsymbol{\omega}\times\boldsymbol{v})_i] + \frac{\partial^2}{\partial x_i^2}\left(\rho_0\frac{|\boldsymbol{v}|^2}{2}\right) \quad (1)$$

where ρ_0 and c_0 are the density of the fluid and the speed of sound at the listener's position $\boldsymbol{x}$, respectively, p' is the acoustic pressure perturbation, $\boldsymbol{v}$ is the velocity, and $\boldsymbol{\omega}=\nabla\times\boldsymbol{v}$ is the vorticity. The acoustical density perturbation ρ' has been neglected with respect to the mean density ρ_0 in the right-hand side of Eq. (1) as a consequence of the low Mach number approximation in the source region. (That is equivalent to the assumption of compactness of the acoustic source.)

The acoustical pressure perturbation p' is obtained by integration of Powell's[12] analogy (1) using a suitable Green's function (see Ref. 15). In absence of surfaces, the second term in the right-hand side of Eq. (1) yields a monopolar contribution to the far field, proportional to the second time derivative of the total kinetic energy of the flow. We consider here an incompressible and homentropic flow in the source region, for which kinetic energy is a conserved quantity, so that the second term in the right-hand side of Eq. (1) does not contribute to the acoustical field. Moreover, in absence of external forces, the total impulse of the flow is conserved as well. In these conditions, the leading-order term of the sound field is a quadrupole as shown by Lighthill,[3] despite the dipole that is apparently indicated by the divergence operator in $\nabla\cdot[\rho_0(\boldsymbol{\omega}\times\boldsymbol{v})]$. As stressed by Crighton,[16] the fact that the quadrupolar source is hidden in the dipole of Powell's source term[12] can lead to severe overestimates of the sound prediction when the sound producing mechanism is not clearly identified. Powell's analogy offers nevertheless a convenient framework for the prediction of the sound generated by vortical flows.

Powell and Möhring Analogies

Assuming the conservation of momentum and kinetic energy and using the free-field Green's function (see Ref. 15), Powell[12] obtains the integral formulation

$$p'(\boldsymbol{x},t) = -\frac{\rho_0}{4\pi c_0^2|\boldsymbol{x}|^3}\frac{\partial^2}{\partial t^2}\iiint_V (\boldsymbol{x}\cdot\boldsymbol{y})\boldsymbol{x}\cdot(\boldsymbol{\omega}\times\boldsymbol{v})\,\mathrm{d}^3\boldsymbol{y} \quad (2)$$

where $\boldsymbol{y}$ is a point in the source region. The integrand has to be evaluated at the retarded time $t-|\boldsymbol{x}|/c_0$, and the integration volume V extends over the region of nonvanishing vorticity.

An advantage of vortex sound theory is that vorticity dynamics provides an efficient description of an inviscid incompressible flow. Furthermore, the vorticity is limited in space compared to the velocity so that the integration domain in the vortex sound analogy can be much smaller than for Lighthill's analogy.

Möhring[11] derives another formulation of the vortex sound analogy using Helmholtz's vorticity equation for inviscid incompressible flows:

$$\frac{\partial\boldsymbol{\omega}}{\partial t} + \nabla\times(\boldsymbol{\omega}\times\boldsymbol{v}) = 0 \quad (3)$$

and a vectorial Green's function. Assuming once more the conservation of kinetic energy, Möhring obtains an expression that does not depend explicitly on the velocity $\boldsymbol{v}$:

$$p'(\boldsymbol{x},t) = \frac{\rho_0}{12\pi c_0^2|\boldsymbol{x}|^3}\frac{\partial^3}{\partial t^3}\iiint_V (\boldsymbol{x}\cdot\boldsymbol{y})\boldsymbol{x}\cdot(\boldsymbol{y}\times\boldsymbol{\omega})\,\mathrm{d}^3\boldsymbol{y} \quad (4)$$

where the integrand has again to be evaluated at the retarded time $t-|\boldsymbol{x}|/c_0$. Apart from the additional assumption of conservation of the kinetic energy made by Möhring, formulations (2) and (4) are equivalent.[17,18] However, because of the three time derivatives in Eq. (4) instead of the two time derivatives in Eq. (2), the application of Möhring's analogy[11] seems more sensitive to noise. Nevertheless, it appears that Möhring's form is more robust than Powell's formulation.[12] This is because that Möhring's formulation corrects for the variation of kinetic energy induced by the noise in the experimental or theoretical data used.

To illustrate this, we consider the leapfrogging of two vortex rings. We use the blob model of Kambe and Minota.[13] The key idea is to explore the sensitivity of the predicted sound field to random errors added to the solution of the flowfield used as input for the integral formulation.

The initial characteristics of the vortex rings considered have been defined on the basis of our particle image velocimetry measurements shown later. The initial spacing between the vortices is half the initial diameter, and the initial core size is about 1/10th of the initial ring diameter (see the Appendix). The circulation of each vortex is equal to $0.55U_0D$. The trajectory of the vortices has been integrated over 100 points covering one cycle. A small-amplitude white noise (zero mean value, standard deviation equal to 10^{-5}) has been added to the radial and axial coordinates of each of the vortex blobs independently to evaluate the respective robustness of Möhring[11] and Powell[12] formulations.

For the unperturbed evolution of the vortex rings, it can be seen in Fig. 1 that the acoustical source terms obtained using Powell's source term[12]

$$q_P \equiv -\frac{\partial^2}{\partial t^2}\iiint_V (\boldsymbol{x}\cdot\boldsymbol{y})\boldsymbol{x}\cdot(\boldsymbol{\omega}\times\boldsymbol{v})\,\mathrm{d}^3\boldsymbol{y} \quad (5)$$

and Möhring's source term[11]

$$q_M \equiv 3\frac{\partial^3}{\partial t^3}\iiint_V (\boldsymbol{x}\cdot\boldsymbol{y})\boldsymbol{x}\cdot(\boldsymbol{y}\times\boldsymbol{\omega})\,\mathrm{d}^3\boldsymbol{y} \quad (6)$$

are equal. (The listener's position $\boldsymbol{x}$ is set at a unit distance on the axis of symmetry.) The peak sound emission occurs at the phase of the leapfrogging for which the vortices are coplanar.

Figure 2 shows the difference between the acoustical source terms calculated using the perturbed vortex coordinates and the unperturbed ones:

$$\epsilon_{\mathrm{ac}} = q_{\mathrm{perturbed}} - q_{\mathrm{unperturbed}} \quad (7)$$

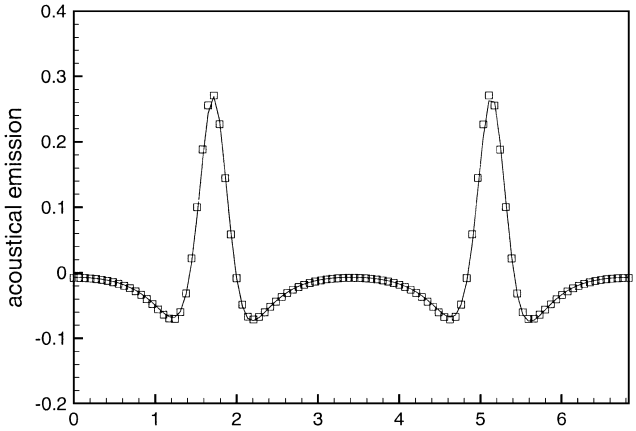

Fig. 1 Acoustical emission of vortex leapfrogging: ——, Powell's source term (5) and □, Möhring's source term (6).

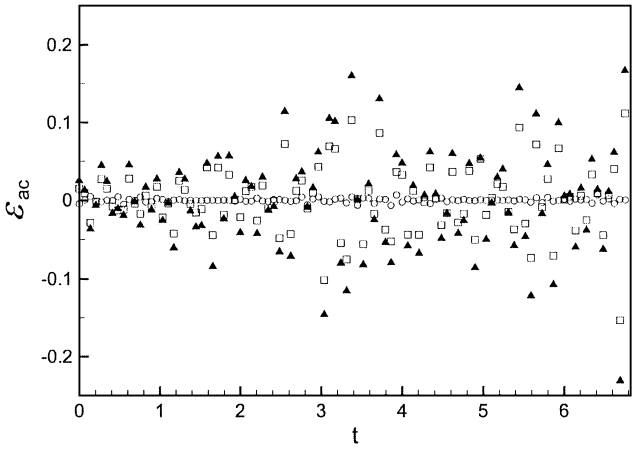

Fig. 2 Difference between the acoustical emission obtained from the perturbed and the unperturbed vortex rings evolution: ▲, Powell's source term (5); □, Möhring's source term (6); and ○, conservative source term (19).

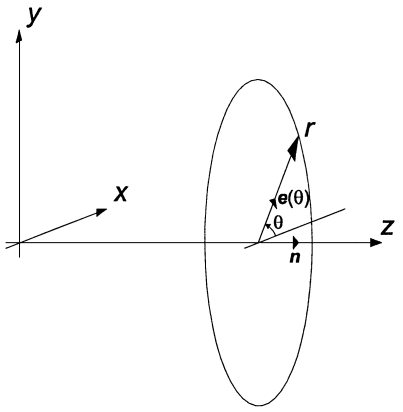

Fig. 3 Axisymmetrical coordinates system.

It appears that in spite of its additional time derivative, Möhring's[11] formulation (4) is indeed slightly more robust than Powell's form (2) for this type of perturbation. A more detailed discussion is provided in an earlier paper[10] in which we show that an additional improvement of the prediction is obtained by correction for the fluctuations of the trajectory z_0 of the center of gravity of the vorticity. We discuss this correction again in the next section.

Conservative Formulation for Axisymmetrical Vortical Flows

In this section, we generalize the approach followed by Möhring[11] to predict the sound produced by two leapfrogging vortex filaments to the case of a continuous distribution of vorticity.

We consider a flow that has a cylindrical symmetry. The coordinate of an element of vorticity is given by

$$\boldsymbol{y} = z\boldsymbol{n} + r\boldsymbol{e}(\theta) \tag{8}$$

where $\boldsymbol{n}$ and $\boldsymbol{e}(\theta)$ are unit vectors parallel with and perpendicular to the axis of symmetry, respectively (Fig. 3). We adopt here the same formalism as used by Möhring.[11] The vorticity and velocity are expressed by

$$\boldsymbol{\omega}(r, \theta, z) = \boldsymbol{\omega}(r, z)\boldsymbol{n} \times \boldsymbol{e}(\theta)$$

$$\boldsymbol{v}(r, \theta, z) = u(r, z)\boldsymbol{n} + v(r, z)\boldsymbol{e}(\theta) + w(r, z)\boldsymbol{n} \times \boldsymbol{e}(\theta)$$

Substituting this description of the flow into Möhring's expressions (4) yields

$$p'(\boldsymbol{x}, t) = \frac{\rho_0}{4c_0^2|\boldsymbol{x}|^3}\frac{\mathrm{d}^3 Q}{\mathrm{d}t^3}\boldsymbol{x} \cdot \left(\boldsymbol{nn} - \frac{\boldsymbol{I}}{3}\right) \cdot \boldsymbol{x} \tag{9}$$

where Q is defined by

$$Q \equiv \iint_S \omega r^2 z \mathrm{d}r\, \mathrm{d}z \tag{10}$$

We use the expressions of the impulse P and kinetic energy T for rotational incompressible flow,[19]

$$P = \frac{\rho_0}{2}\iiint_V \boldsymbol{y} \times \boldsymbol{\omega}\, \mathrm{d}^3\boldsymbol{y} \tag{11}$$

$$T = \rho_0 \iiint_V \boldsymbol{y} \cdot (\boldsymbol{\omega} \times \boldsymbol{v})\mathrm{d}^3\boldsymbol{y} \tag{12}$$

that become in the axisymmetric case[20]

$$P = \pi\rho_0 \iint_S \omega r^2 \mathrm{d}r\, \mathrm{d}z \tag{13}$$

$$T = 2\pi\rho_0 \iint_S (ru - zv)\omega r\, \mathrm{d}r\, \mathrm{d}z \tag{14}$$

When the conservation of the impulse is assumed, it can be demonstrated by straightforward algebra that the time derivative of Möhring's[11] integrand can be related to the kinetic energy:

$$\frac{\mathrm{d}Q}{\mathrm{d}t} = \frac{T}{2\pi\rho_0} + 3\iint_S \omega v r z\, \mathrm{d}r\, \mathrm{d}z \tag{15}$$

so that

$$\frac{\mathrm{d}^3 Q}{\mathrm{d}t^3} = \frac{\mathrm{d}^2}{\mathrm{d}t^2}\left(3\iint_S \omega v r z\, \mathrm{d}r\, \mathrm{d}z\right) \tag{16}$$

which is the expression used by Möhring based on the kinetic energy conservation $\mathrm{d}T/\mathrm{d}t = 0$.

Similarly, it can be shown that Powell's[12] integral in Eq. (2), rewritten using index notation as

$$\iiint_V (\boldsymbol{x} \cdot \boldsymbol{y})\boldsymbol{x} \cdot (\boldsymbol{\omega} \times \boldsymbol{v})\mathrm{d}^3\boldsymbol{y} = x_i x_j \iiint_V y_i(\boldsymbol{\omega} \times \boldsymbol{v})_j\, \mathrm{d}^3\boldsymbol{y} \tag{17}$$

has a trace equal to $T|\boldsymbol{x}|^2/\rho_0$. This contribution, which vanishes in the further time derivations assuming the conservation of kinetic energy, therefore, can be dropped from Powell's source term. This illustrates that the correction of the source term based on the assumption of conservation of the kinetic energy can be applied not only for axisymmetrical cases but also for more general problems.[21]

An additional correction is the substraction of an axial center of gravity of the vortex system z_0 defined as[20]

$$z_0 \equiv \frac{\iint_S \omega r^2 z\, \mathrm{d}r\, \mathrm{d}z}{\iint_S \omega r^2\, \mathrm{d}r\, \mathrm{d}z} = \pi\rho_0\frac{Q}{P} \tag{18}$$

from the axial coordinate z in the integral source term of Eq. (15),

$$\frac{\mathrm{d}Q}{\mathrm{d}t} = \frac{T}{2\pi\rho_0} + 3\iint_S \omega v r (z - z_0)\, \mathrm{d}r\, \mathrm{d}z \tag{19}$$

Expressions (15) and (19) are equivalent because

$$\iint_S \omega v r (z - z_0)\, \mathrm{d}r\, \mathrm{d}z = \iint_S \omega v r z\, \mathrm{d}r\, \mathrm{d}z - \frac{z_0}{2\pi\rho_0}\frac{\mathrm{d}P}{\mathrm{d}t} \tag{20}$$

in which we assume once more the conservation of impulse.

Hence, when once more the conservation of the impulse and of the kinetic energy is assumed, Möhring's analogy (4) can be rewritten in the form

$$p'(\boldsymbol{x}, t) = \frac{3\rho_0}{4c_0^2|\boldsymbol{x}|^3}\frac{\mathrm{d}^2}{\mathrm{d}t^2}\left[\iint_S \omega v r (z - z_0)\, \mathrm{d}r\, \mathrm{d}z\right]\boldsymbol{x} \cdot \left(\boldsymbol{nn} - \frac{\boldsymbol{I}}{3}\right) \cdot \boldsymbol{x} \tag{21}$$

in which only two time derivatives of an integral quantity are required to calculate the sound radiated. It can be shown by straightforward algebra that the same corrections for momentum conservation, energy conservation, and for the path of the center of gravity z_0 applied to Powell's analogy (2) lead to the same final equation (21) (Ref. 10).

Note that any definition of z_0 that does not depend on the space coordinates would equally guarantee the equivalence of the expressions (15) and (19). Subtracting the coordinate of a center of gravity of the vorticity distribution to the coordinate z of each element of vorticity presents the following advantage. In our case, the vortices are convected in the axial direction, so that the noise that affects the vorticity, velocity, and coordinates of the vortex rings is multiplied in the integral of Eq. (15) by an axial coordinate z that grows continuously. This degrades more and more the differentiability of Eq. (15) as the vortices are convected downstream. Subtracting the axial coordinate of a center of gravity to z in the integrand of Eq. (15) presents, therefore, the advantage that the amplitude of the noise on the integrand remains bounded.

It appears that the particular form of z_0 defined by Eq. (18) improves significantly the numerical stability of the sound prediction.[10] Figure 2 shows that the sound predicted by the conservative formulation using as an input the perturbed evolution of the leapfrogging vortex rings described earlier is very close to the sound predicted from the unperturbed data.

Prediction of the Sound Produced by Vortex Pairing in a Subsonic Jet

In what follows, we shall not consider the sound radiated by asymmetric interactions such as the ones that take place between elliptic rings,[8,22] or in azimuthally unstable rings.[23,24]

So far, the prediction of the pairing phenomenon has been based on theoretical and/or numerical descriptions of the flowfield. Depending on the modeling of the vortex rings, their mutual Biot–Savart interaction (vortex leapfrogging) or their actual coalescence into one single ring (vortex merging) can be simulated.

When the core thickness of the rings is small compared to the initial axial separation d between the rings, which is itself small compared to the rings radii R, the rings can be modeled as filaments and the leapfrogging is locally described as a two-dimensional plane flow. The sound produced by such a model has been predicted by Möhring[11] applying his formulation of the vortex sound theory. If the initial separation d is not negligible compared to the rings radii R, the vortex stretching and the resulting modulation of the rings self-induced velocity have to be taken into account. Dyson's[25] axisymmetrical vortex interaction model has been used by Kambe and Minota[13] to predict the sound radiated by the corresponding periodic leapfrogging of the vortex rings. They predicted that the sound emitted is maximum at the moment at which the rings are coplanar. Shariff et al.[26] showed that by improving Dyson's model to allow the ring cores to be strained into ellipses, a high-frequency noise component is added to the low-frequency component associated to the period of leapfrogging.

To simulate the merging of the rings, the flow model must permit the deformation of the ring cores. Using contour dynamics to simulate a range of vortex ring interactions (mutual slip-through, coalescence, etc.), Tang and Ko[27] investigated in detail the sources of the low and high frequencies that they observed in the sound radiated. They showed that the sound produced by the mutual slip-through and coalescence of the vortex rings can be related to the axial rate of acceleration and radial acceleration of the vortex ring centroids. Using an incompressible axisymmetric direct numerical simulation for the calculation of the vortex rings dynamics, Verzicco et al.[14] confirmed the presence of the higher frequency in the sound generated for some initial vortex ring configuration, which they identify as the eddy turnover frequency.

Subsonic Excited-Jet Facility

The experimental facility is shown in Fig. 4. A nozzle is connected to a 0.9-m^3 wooden settling chamber by means of a 1.7-m-long straight cylindrical pipe. Air enters into the pipe through a honeycomb, and turbulence is further reduced by grids placed just upstream of the nozzle. The shape of the contraction is based on a seventh-order polynomial that ensures the outlet flow uniformity and low-turbulence level (below 0.3% in a range of outlet velocity from 5 to 40 m/s). It also avoids separation of the laminar boundary

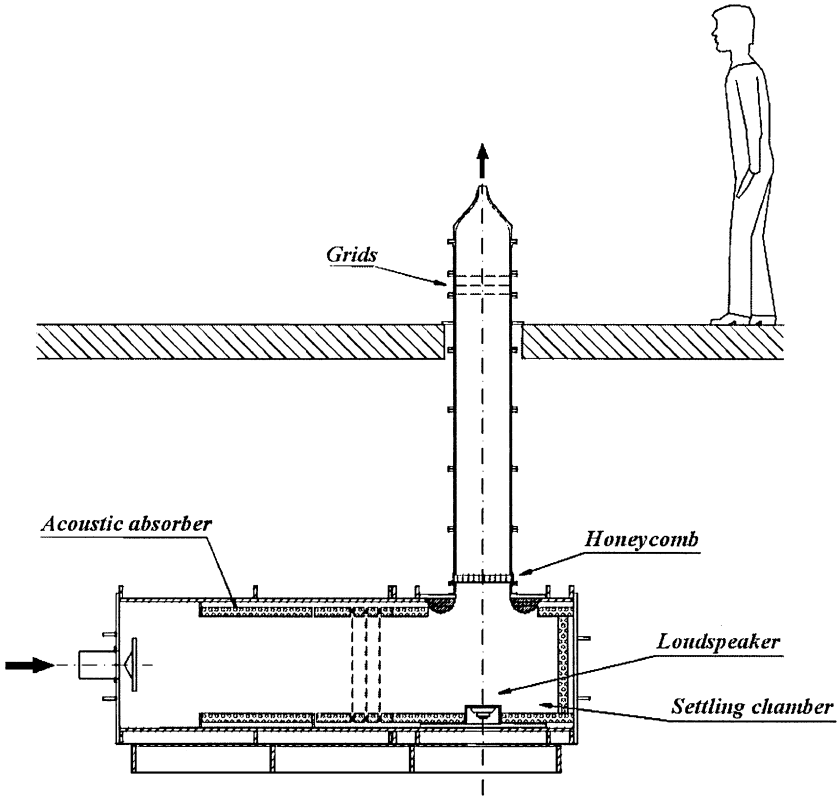

Fig. 4 Experimental facility.

layer. The contraction ratio is 56. The outlet diameter D is 0.041 m. The walls of the settling chamber are covered with a 10-cm layer of acoustical absorbing foam to reduce acoustical resonances of the settling chamber. The acoustical behavior of the setup is dominated by the resonant modes of the pipe and nozzle. The air is supplied to the settling chamber by an ejector connected to a 7-bar compressed air network. The jet instability is forced using a loudspeaker placed at the bottom of the settling chamber, on the nozzle axis.

Pseudo-Time-Resolved Particle Image Velocimetry Measurements

The flow is seeded at the entrance of the settling chamber with particles obtained by evaporation of oil on a heated plate followed by recondensation. A uniform seeding across the shear layer is obtained by operating the jet with a large seeding density for approximately 10 min to seed the $4 \times 3 \times 4\ \mathrm{m}^3$ room hosting the jet. The jet seeding density is then reduced to match the room seeding density.

The diameter of the particles is estimated to be of the order of 1 μm. A meridian plane of the jet flow is illuminated by a laser sheet provided by a Nd:YAG laser firing pairs of 5-ns duration pulses at a frequency that can be tuned between 8 and 12 Hz. The particle images are recorded by a 12-bit fan-cooled digital PCO SENSICAM® camera having a full frame resolution equal to (1280×1024) pixel^2. The images are acquired by a personal computer-mounted frame grabber and software PCO SENSICONTROL®, synchronized at half the laser frequency.

The particle images are processed using particle image velocimetry (PIV) software, Window Distortion Iterative Multigrid (WIDIM)[28] developed at the von Kármán Institute. The data analysis is based on the cross correlation of the pairs of images acquired at the successive instants corresponding to the pairs of laser pulses.

Stroboscopic PIV measurements[29] have been performed to obtain pseudo-time-resolved acquisitions of the vortex pairing. The PIV snapshots are slightly desynchronized with respect to a submultiple of the acoustical excitation frequency, so that the aliasing effect results in an apparent slow motion during the evolution of the measured vortex pairing. The pseudotime delay between two PIV acquisitions is obtained by the relationship

$$\Delta t_s = \mathrm{mod}(1/f_p, 1/f_e) \tag{22}$$

where f_P and f_e are the PIV triggering and acoustical excitation frequencies, respectively.

Measurements have been performed for a jet outlet velocity of $U_0 = 5.0$ m/s. PIV images have been acquired with a large field of view to characterize the overall evolution of the flow during pairing. The PIV acquisition and processing parameters are summarized in Table 1. The indicated spatial resolution is based on the size of the interrogation windows, irrespective of the overlap.

Table 1 Experimental conditions and PIV measurements

Condition	Measurement
Experimental conditions	
Nozzle outlet velocity	$U_0 = 5.0$ m/s
Excitation frequency	$f_e = 114$ Hz
Excitation Strouhal	$Sr = 0.93$
Excitation amplitude	$u'_e/U_0 = 0.2\%$
PIV acquisitions parameters	
Field of view	x: $4.2D$, y: $2.4D$
Image size	[1280, 768] pixel
Calibration	0.13322 mm/pixel
Pulse separation	100 μs
Acquisition frequency	4.062 Hz
Number of acquisitions	10×32 images
PIV processing parameters	
Final window size	[12, 12] pixel
Final window overlap	[6, 6] pixel
Spatial resolution	1.6 mm $\simeq D/26$

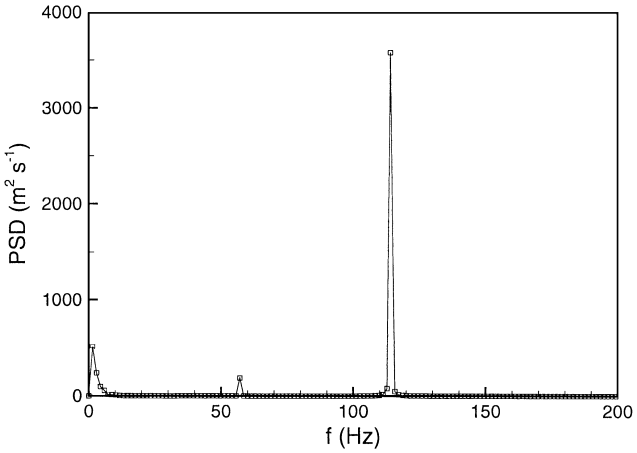

Fig. 5 Power spectral density of the excitation acoustical velocity in the nozzle outlet plane.

The jet is harmonically excited at a frequency $f_e = 114$ Hz, corresponding to the quarter-wavelength mode of the pipe-nozzle resonator. The corresponding excitation Strouhal number is

$$Sr_D = f_e D/U_0 = 0.93 \tag{23}$$

For the stroboscopic (pseudo-time-resolved) PIV measurements, the PIV triggering frequency is set to $f_P = 4.062$ Hz. The stroboscopic acquisition frequency, equal to the inverse of the Δt_s calculated using Eq. (22), is $f_s = 1754$ Hz. The amplitude of the excitation is defined by

$$a_e \equiv u'_e/U_0 \tag{24}$$

where u'_e is the standard deviation of the harmonic velocity fluctuation at the exit plane of the nozzle on its centerline. We have $a_e = 0.2\%$ for the present measurements. These values are summarized in Table 1. More details on the flow conditions and excitation parameters are given by Schram.[30] The velocity perturbation is used further as a reference to determine the phase of the PIV data. Figure 5 shows the power spectrum of the velocity perturbation u'_e. Aside from a weak subharmonic at 57 Hz, the frequency of the velocity perturbation signal is seen to be quite concentrated at 114 Hz. The phase φ at which the PIV acquisitions are performed is determined using a data acquisition board that samples both the PIV synchronization signal S_P and the loudspeaker excitation signal S_l. Before and after each PIV measurement series, simultaneous acquisitions of the loudspeaker excitation signal S_l and the acoustical velocity perturbation in the nozzle outlet plane S_u (measured by hot-wire anemometry) have been performed. The phase lag between both signals is obtained by cross correlation, so that the phase φ of each PIV measurement can be known with respect to the acoustical velocity perturbation signal S_u. A jitter of 1% of the phase lag between S_l and S_u has been observed. This jitter can be partly explained by the variation of the speed of sound $c = \sqrt{(\gamma RT)}$ inside the pipe due to variations of the air temperature T (for fixed gas properties $\gamma = 1.4$ and $R = 287$ J/kg K). Temperature fluctuations of the order of 0.5 K have been measured over the duration of a PIV measurement series. The accuracy of the detection of the phase is 1% (Ref. 31).

Processing

PIV Processing: Accuracy vs Robustness

When the robustness of the sound prediction based on the measured flowfield is considered, the spatial integration that is applied in the analogies (2), (4), or (21) is favorable, but the multiple-time derivatives that have to be subsequently applied are unfavorable. Hence, it seems appropriate to obtain a smooth description of the temporal and spatial evolution of the flowfield.

In PIV, smooth data are obtained using large interrogation windows. However, because of the spatial averaging effect of PIV, such

an approach is detrimental to the accuracy and leads to a systematic underestimation of the peak vorticity. Using small interrogation windows increases the cutoff frequency of the low-pass PIV filter, but leads to less reliable measurements. Indeed, the number of particle images contained within an interrogation window is an essential parameter determining the signal-to-noise ratio of the correlation. This problem is particularly crucial in the core of the vortex ring, where the particle density decreases because of centrifugation. PIV software based on iterative multigrid algorithms such as the one used in this work are necessary to decouple the resolution and the accuracy.

Vorticity

Two different approaches have been tested for the calculation of the vorticity from the velocity fields. The first approach is based on finite difference schemes, for which the truncation error is well known, but that are also known to amplify the measurement noise. The second approach is aimed at reducing high-frequency noise and is based on the local fit of the velocity field by means of analytical functions. The derivative of the data are then calculated from the analytical derivative of the fit function, so that the accuracy is the one with which the fitted coefficients are obtained.[32]

It has been observed[31] that although the second approach provides smoother vorticity fields than the finite difference schemes, the difference vanishes in the spatial integration of the vorticity field used in our analogy (Fig. 6). The third-order accurate Richardson scheme has, thus, been chosen for the calcuation of each instantaneous vorticity field. The vorticity fields have not been subjected to any smoothing method. The adequacy of the spatial sampling has been assessed on the basis that the vorticity fields obtained using different magnifications were quite similar, in particular regarding the value of the peak vorticity.

The uncertainties on the velocity and on the vorticity have been evaluated following the procedure indicated previously.[29] We found that the relative uncertainty on the velocity is below 1.5% and the one on the vorticity is below 6.5%.

Integration Domain

As already introduced, measurements have been taken over a large field of view that covers the region over which pairing occurs. As a result, a given instantaneous field comprises vortices that are pairing, but also vortices that are still emerging from the shear layer and vortices that result from a previous merging. An important step in the processing is, thus, the isolation of the pairing vortices. Because an important amount of data is needed to obtain reliable statistics, a minimum of user intervention is required by such a process.

An automatic vortex detection algorithm, based on the continuous wavelet transform[29] has been used. The isotropic Mexican hat wavelet has been chosen for its similarity with the Gaussian vorticity patterns that is postulated for our vortices. Some outputs of this method are the localizations and sizes of the vortex cores. In particular, the core radius is defined as the distance from the core center at which the tangential velocity reaches its maximum value. The sampling requirement of the Mexican hat is such that the smallest vortex that can be detected by our procedure has about four data points across its core diameter.

This algorithm involves an analytical calibration using as a prototype vortex the Oseen vortex model, characterized by a Gaussian vorticity profile. The relevance of this vortex model can be assessed on the basis of Fig. 7, which shows that the profile of vorticity across the vortex cores exhibits a Gaussian pattern. The limitation of our method is its inability to characterize the ellipticity of the vortex core: Nonisotropic vortices can be detected, but the size that is given is averaged over all directions in the measurement plane. However, this is not a problem in the present case, for which the integration domain comprises a larger region around the vortex cores.

Hence, the method used to clean the fields consists in the following steps: 1) detecting (and sizing) the vortex cores, 2) selecting in an initial field of the vortices that are participating in the pairing process, and 3) tracking of these vortices during pairing and cancellation of the velocity and vorticity at grid points that are not located within a window centered on the vortices.

By considering the conservation of circulation, we found that a rectangular window as shown in Fig. 8 provides the best results. The center of the rectangular domain follows the average axial position of the two vortices indicated by the wavelet detection algroithm. Experiments with circular windows attached to the vortices in combination with a thresholding criterion for the magnitude of the vorticity appeared to be less robust. In particular, there was a significant discontinuity in the size of the integration domain during the transition from two distinct vortex rings to one single merged vortex ring.

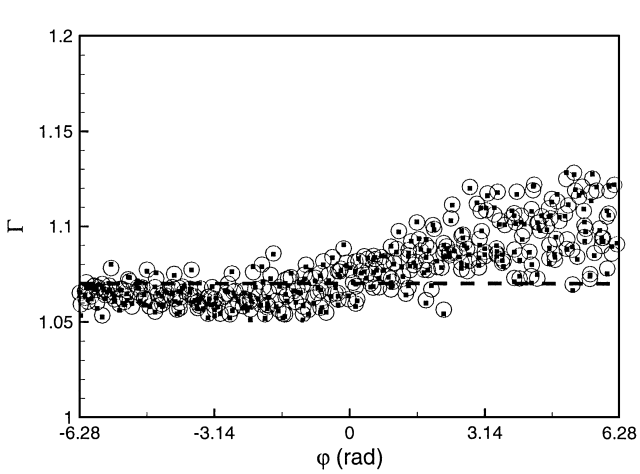

Fig. 6 Total circulation of the two pairing vortices, normalized as indicated in Table 2: ■, vorticity calculated using third-order-accurate Richardson scheme; ○, vorticity calculated using analytical fit; and – – –, theoretical prediction (26).

Realignment of the System of Coordinates

To use the PIV data into the acoustic analogy, it matters that the PIV system of coordinates (x, y) is correctly aligned with the system of axes (z, r) of the axisymmetric jet. It is here assumed that the acoustical excitation forces the axisymmetric varicose mode of the jet and that the sinuous or spinning modes are negligible. The remaining source of misalignment might also be the inaccurate positioning of the camera with respect to the jet aerodynamic axis of symmetry. This issue has been considered on the basis of the localizations of the vortices obtained from the wavelet analysis. Figure 9 shows the locus of the vortices that have been detected among 320 fields acquired in large field of view. The aerodynamical axis of the jet has been obtained by averaging the polynomial fits of the trajectories of the upper and lower cores. We observed a systematic shift of the axis by $y/D = -0.005$. We corrected for this shift. To compensate for a residual misalignment between the axis of the vortex rings and the measurement axis, we perform the average of the quantities integrated over each side $y < 0$ and $y > 0$ of the PIV fields.

Results

Figure 10 shows the evolution of the vorticity field during one period of pairing. Because the pairing involves two vortex rings, the pairing process lasts two acoustical excitation periods. The phase φ of the PIV fields that compose each series has been shifted by a value of $2\pi/3$ so that the phase at which the vortices are coplanar corresponds to $\varphi \simeq 0$ rad.

The results to be discussed concern at first the conservation of the circulation and the impulse and the kinetic energy of the system constituted by the two pairing vortices. The prediction of the radiated sound follows in the next subsection. These results have been obtained using a normalization based on the nozzle outlet diameter D and the outlet velocity U_0. The corresponding scaling for the different quantities is indicated in Table 2. The quantities that will be shown result from the averaging of the integrations performed on each side of the symmetry axis.

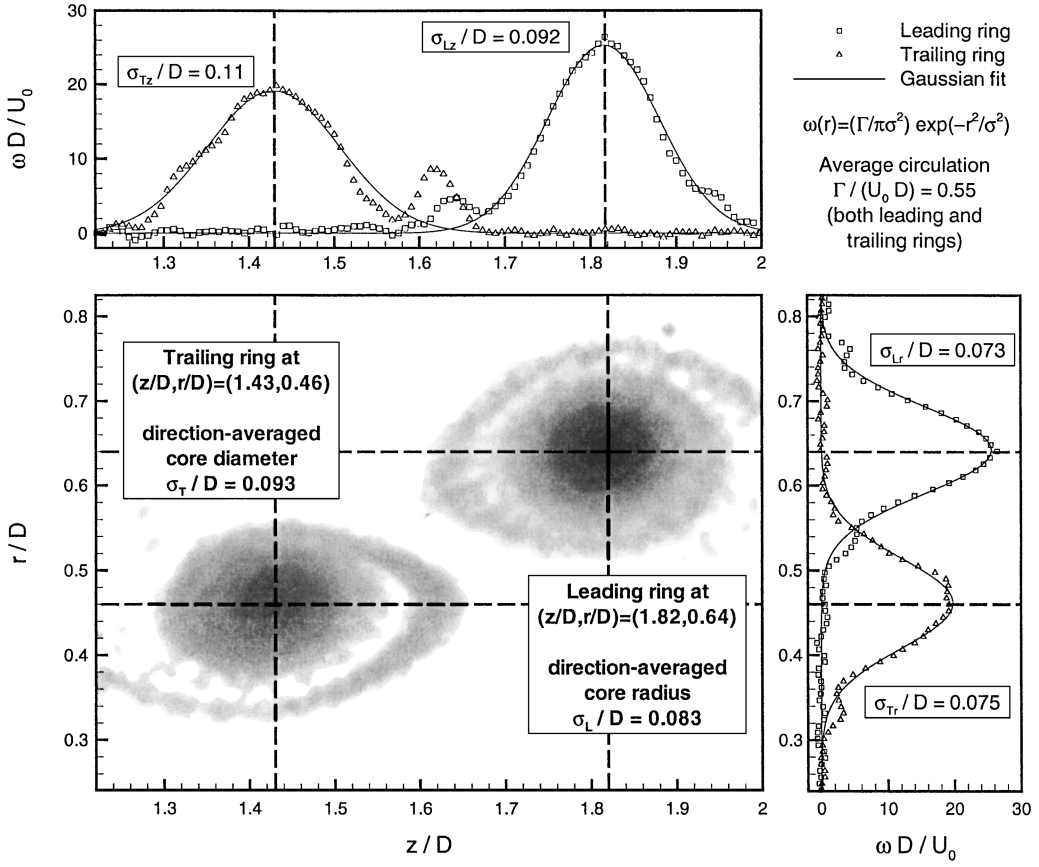

Fig. 7 Initial characteristics of the leading and trailing vortex rings obtained from the PIV measurements, where σ_{Lr} and σ_{Lz} are the core radii of the leading ring in the radial and axial directions and σ_{Tr} and σ_{Tz} are the corresponding core radii of the trailing ring: gray-level contours, vorticity; symbols, vorticity profiles; and ——, Gaussian fit.

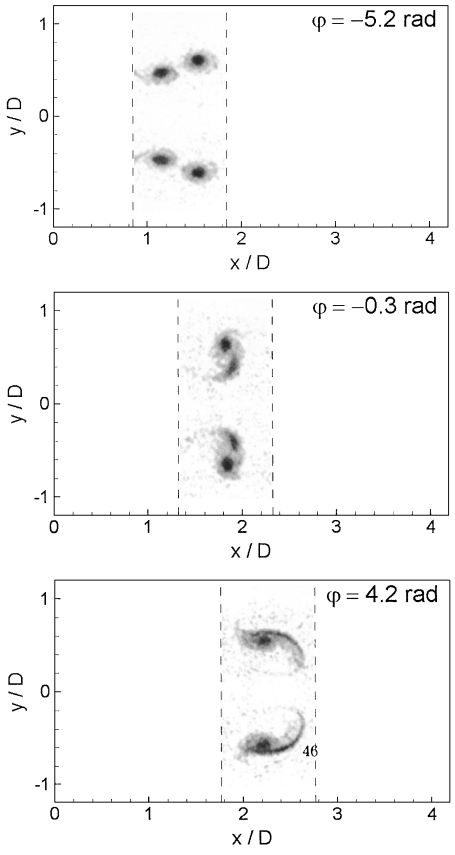

Fig. 8 Vorticity field of the two pairing vortices, bounded by the moving integration window.

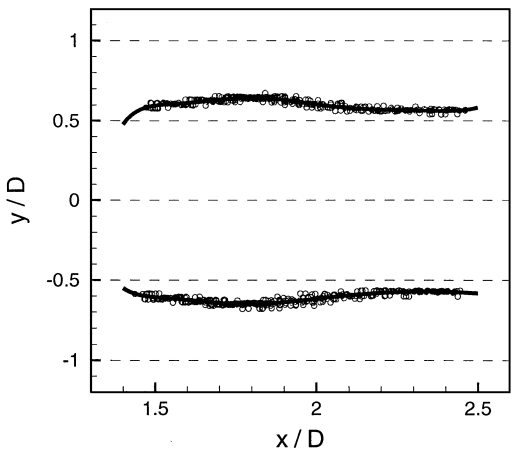

Fig. 9 Localization of the leading and merged vortex rings.

Flow Invariants

The circulation is here obtained by integration of the vorticity over the domain indicated in Fig. 8. Figure 6 shows that the circulation of the vortex pair is effectively conserved within the scatter in the data for the first acoustical period in the pairing process. In the second acoustical period, we observe an increase of about 10% of the circulation. The magnitude of the circulation can be verified applying a slug model.[33] This model expresses the circulation of a vortex as the amount of circulation that is shed during the period of formation of the vortex. The rate at which circulation is injected into the shear layer is $U_0^2/2$, and the period of formation is $1/f_e$. Thus, we find in dimensional units the summed circulation of two vortices:

$$\Gamma = 2\left(U_0^2/2\right)(1/f_e) \tag{25}$$

and in nondimensional form,

$$\Gamma_{\text{th}} = U_0/Df_e = 1.07 \tag{26}$$

in the present case. Good agreement with this prediction can be observed in Fig. 6.

The longitudinal component of the impulse (per unit density)

$$P = \pi \iint_S \omega r^2 \, \mathrm{d}r \, \mathrm{d}z \tag{27}$$

has been integrated using the same area than for the circulation. Figure 11 shows an apparent growth of about 10% of the impulse during the pairing process, with a slope that increases during the last part of the pairing. The large scatter of the impulse that is apparent in the last part of the pairing phase can probably be attributed to an increasing jitter in the radial coordinates of the vortex cores positions due to growing asymmetric instabilities of the rings. This corresponds to an oscillation of the vortex ring axis of symmetry around its mean value. The evolution of the impulse has also been studied on the basis of its first time derivative directly calculated from the PIV data:

$$\frac{\mathrm{d}P}{\mathrm{d}t} = 2\pi \iint_S \omega v r \, \mathrm{d}r \, \mathrm{d}z \tag{28}$$

(per unit density). The trend exhibited by this derivative (Fig. 12) is quite different from what could be expected from the experimental

Table 2 Normalization of the results

Quantity	Scaling
Vorticity ω	U_0/D
Circulation Γ	$U_0 D$
Impulse P	$U_0 D^3$
Time derivative of the impulse $\mathrm{d}P/\mathrm{d}t$	$U_0^2 D^2$
Kinetic energy T	$U_0^2 D^3$
Acoustic source term Q	$U_0 D^4$
Acoustic source term $\mathrm{d}Q/\mathrm{d}t$	$U_0^2 D^3$
Acoustic source term $\mathrm{d}^3 Q/\mathrm{d}t^3$	$U_0^4 D$

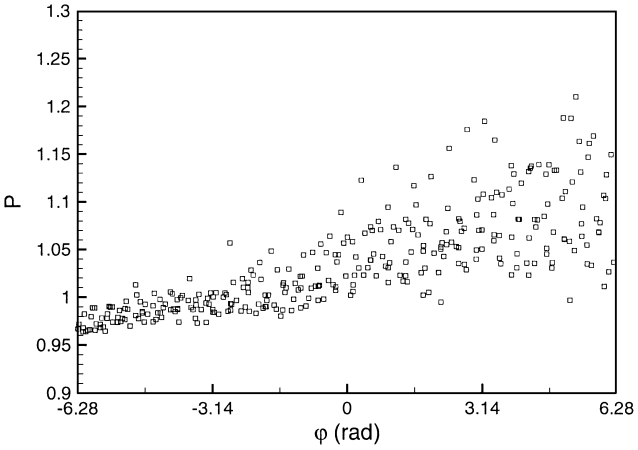

Fig. 11 Total impulse of the two pairing vortices, normalized as indicated in Table 2.

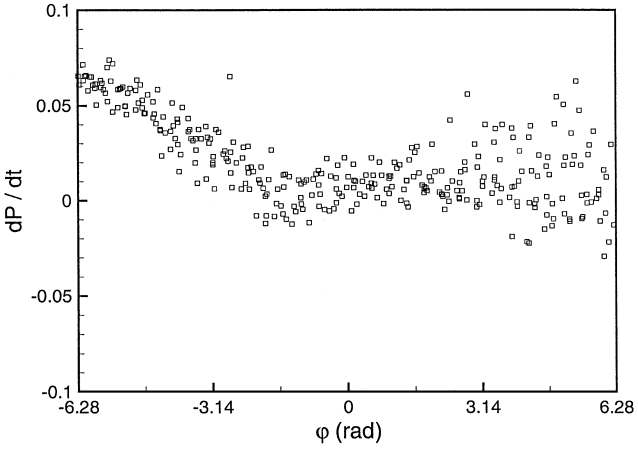

Fig. 12 Time derivative of the total impulse of the two pairing vortices, normalized as indicated in Table 2.

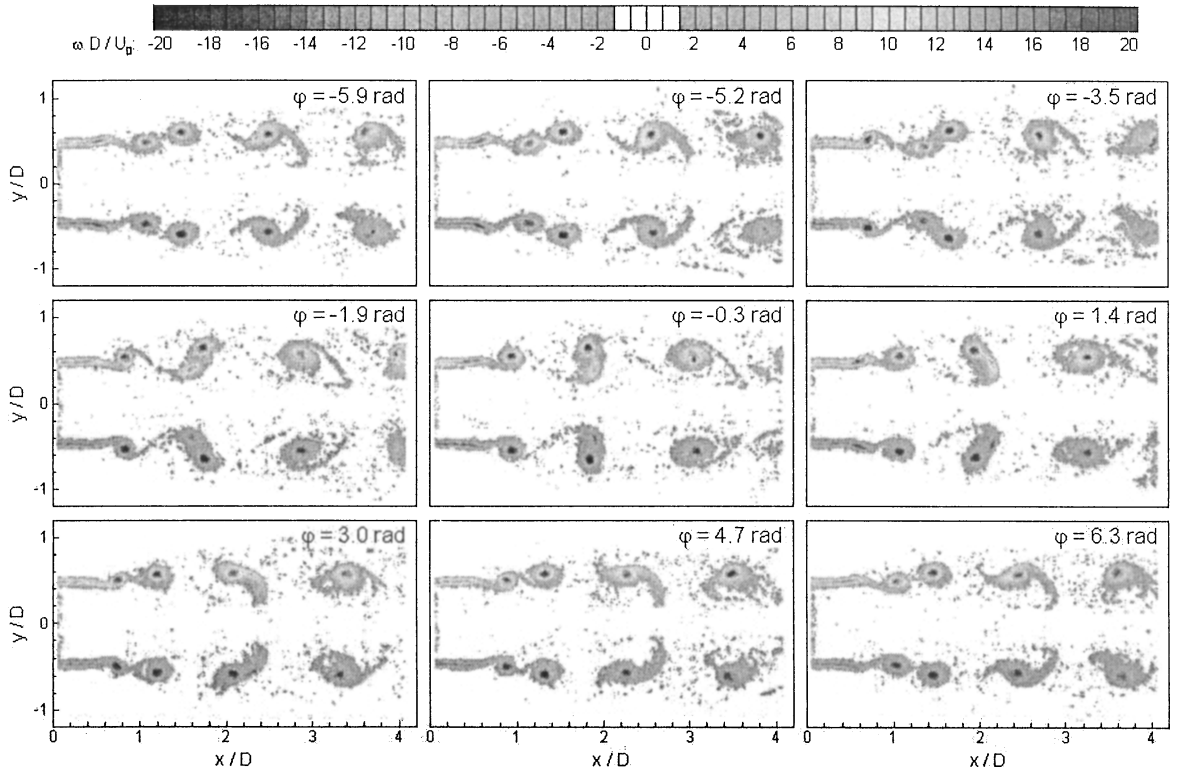

Fig. 10 Temporal evolution of the vorticity field during one sequence of pairing.

data on the impulse (Fig. 11). The slope observed in Fig. 12 decreases from a maximum value during the first part of the pairing and remains slightly positive (about 0.01) during the last part. This discrepancy shows the strong effect of the choice of the formulation on the numerical stability of the results. A physical explanation can be proposed for the trend observed in Fig. 12, based on the knowledge that a variation of the total impulse of a flow region is caused by the application of external forces to this domain.[19] In the present case, these external forces can be attributed to the action of the other vortices that are simultaneously present in the vicinity of the pairing vortices and that have not been taken into account in the integration domain. These vortices are indicated by the numbers 1 and 4 in Fig. 13. Vortex ring 1 is forming in the shear layer and is convected at a velocity that is approximately the same as the mean convection velocity of the pairing vortices 2 and 3. Vortex ring 4 results from a previous merging. Its self-induced convection velocity (proportional to the circulation[19]) is higher than the self-induced velocity of the individual rings before merging.[29] As a result, the contribution of ring 4 to the velocity field at the location of the vortices 2 and 3 is gradually decreasing (dashed line arrow in Fig. 13), whereas the induction of the vortex ring 1 is approximately constant (solid line arrow). This qualitative picture can explain the apparent increase of the total impulse of rings 2 and 3 during the first part of merging because the constant effect of ring 1 is to increase their impulse and the decreasing effect of ring 4 is to reduce their impulse. The increasing separation between the pairing rings and ring 4 and the further instability and breakdown of this ring could explain why the positive slope of $\mathrm{d}P/\mathrm{d}t$ observed in Fig. 12 decreases first with time and then remains slightly positive.

The kinetic energy (14) is plotted in Fig. 14. The impulse can be seen to increase about 10% during the evolution of the pairing vortices, and it also presents more scatter during the last part of pairing.

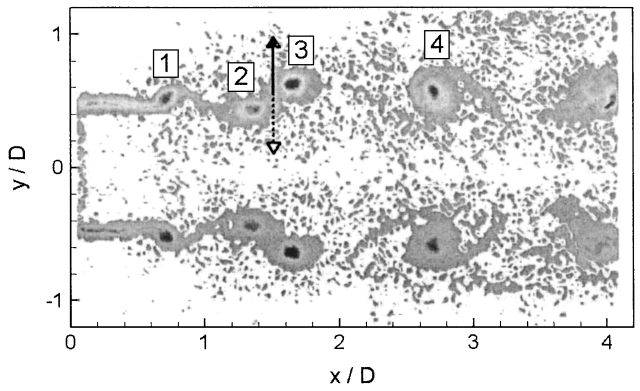

Fig. 13 Distribution of the vortices present in the vicinity of the pairing vortices (extracted from Fig. 10 for the phase $\varphi = -3.5$ rad).

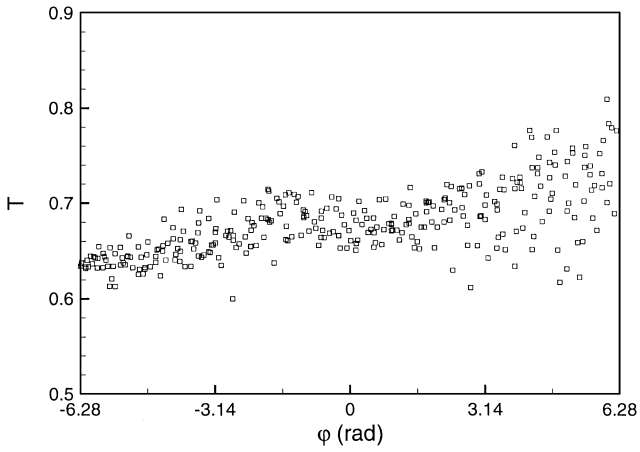

Fig. 14 Total kinetic energy of the two pairing vortices, normalized as indicated in Table 2.

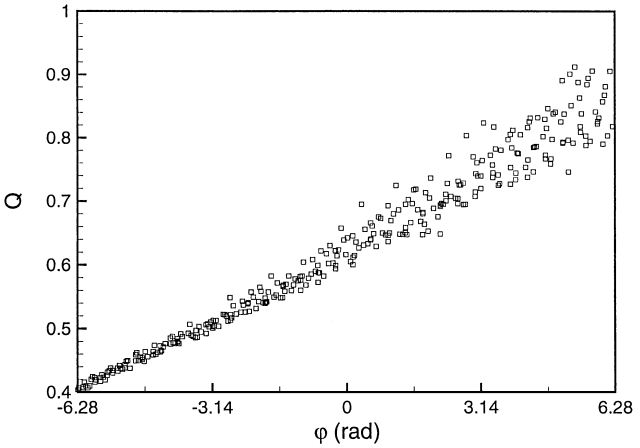

Fig. 15 Möhring's[11] term Q (10) (normalization indicated in Table 2).

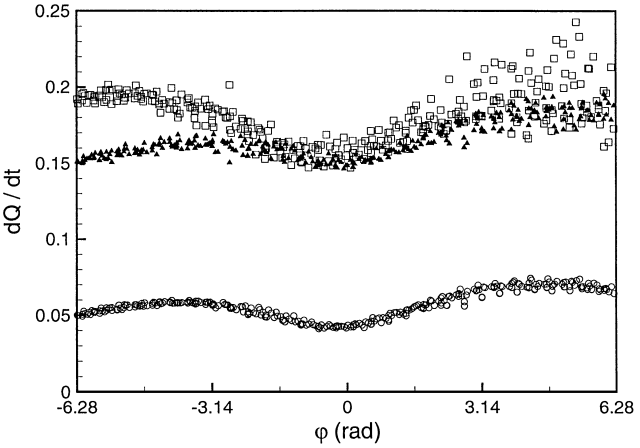

Fig. 16 Acoustic source term $\mathrm{d}Q/\mathrm{d}t$ (normalization indicated in Table 2): □, formulation (15); ▲, formulation (19); and ○, formulation (19) $-T/2\pi\rho_0$.

Acoustic Source Term

Figure 15 shows the acoustical source term calculated using Möhring's[11] expression (10). It can be anticipated that the calculation of the subsequent time derivatives that are required in Eq. (9) will be spoiled by the measurement noise. The first derivative of the acoustical source term $\mathrm{d}Q/\mathrm{d}t$, calculated using Eq. (15), which is shown in Fig. 16, also presents some scatter, but its order of magnitude is much smaller compared to the fluctuation that can be associated to the vortex motion. When formulation (19) is used, which corrects the axial coordinate by subtraction of the vortex centroid z_0, the scatter is even more reduced. Finally, when the kinetic energy term $T/2\pi\rho_0$ (which will vanish in the next time derivative) is subtracted from $\mathrm{d}Q/\mathrm{d}t$, which corresponds to our conservative formulation, the scatter is again reduced. This demonstrates the effectiveness of formulation (19) regarding the robustness of the prediction using a description of the flow that is noisy and/or does not respect the conservation of momentum and kinetic energy. The successive corrections that have been made seem to compensate for the inaccuracies that are inherent to our experimental description of the flowfield. The data points in Fig. 16 identified with circles have to be derived twice with respect to time to yield the acoustical source term. For this purpose, 90 stroboscopic series of 32 PIV fields have been used. The data thereby obtained have been fitted using fourth-order polynomials using overlapping intervals with 95% of overlap, which yields data points every 0.2 rad. The result has been analytically derived twice. The source term $\mathrm{d}^3Q/\mathrm{d}t^3$ is shown in Fig. 17. It indicates that the sound production is maximum when the vortex rings are coplanar, which is in agreement with observations made in Fig. 1 using the vortex blob model of Kambe and Minota.[13] Moreover, it can be seen in Fig. 17 that the peak amplitude obtained

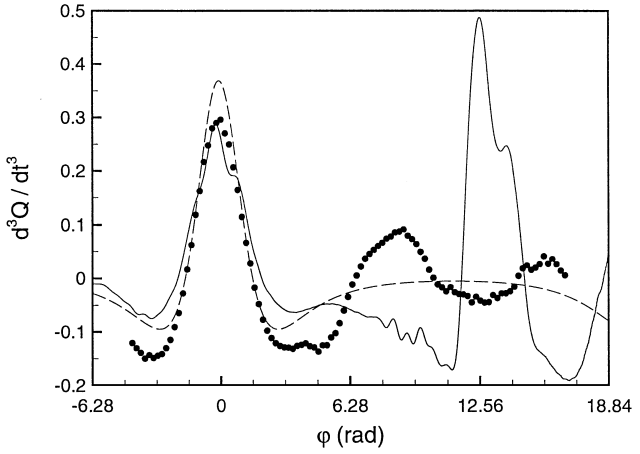

Fig. 17 Acoustic source term d^3Q/dt^3 obtained as follows: ——, numerical simulation; •, experimental data; and – – –, blob model of Kambe and Minota.[13]

using this simplified model matches quite well with the amplitude obtained from the PIV measurements. The sound predicted using the blob model repeats periodically because it does not permit the deformation of the vortex cores that leads to merging.

An incompressible axisymmetric direct numerical simulation of the vortex pairing has been performed to compare the sound prediction obtained experimentally with a sound prediction based on a more realistic description of the flow than on the one obtained from the blob model. The initial conditions have been fixed using the PIV data. (The procedure is provided in the Appendix.) The incompressible Navier–Stokes solver is the one that has already been used by Verzicco et al.[14] to predict the sound radiated by vortex pairing; the numerical aspects are described therein. The sound predicted from the numerical simulation is shown in Fig. 17 arbitrarily shifted in phase to match the moment of pairing observed experimentally. The numerical simulations predicts two peaks of sound production. The first peak corresponds to the leapfrogging of the trailing ring inside the leading one that is also observed from our measurements. The second peak is due to the reciprocal situation, which is not observed from our PIV data in which the vortices merge after the first leapfrogging. Such a discrepancy is most likely due to an inaccuracy in specifying the initial vortex core size ϵ, or the initial separation between the vortex cores d (Appendix), or both. It has indeed been experienced by the authors that the kind of interaction between the vortex rings is strongly influenced by the ratio ϵ/d. The same conclusion has been drawn by Verzicco et al.[14] and Tang et al.[27] Apart from this difference, it can be verified that the agreement between the numerical and the experimental sound predictions is excellent concerning the amplitude of the noise radiated by the first leapfrogging.

Conclusions

The sound produced by vortex pairing has been addressed using a particular form of vortex sound theory. It had been shown previously[10] that Möhring's formulation of vortex sound theory is more robust than Powell's when applied to a noisy description of an axisymmetrical flowfield and that the robustness can be further improved by correcting for the deviation of the path of the vortex system centroid z_0 from a straight path. In our experiments, the scatter in the centroid path z_0 could be due to a low-frequency sinusoidal oscillation of the jet that is not resolved when using the stroboscopic method. Our method allows us to filter out those errors and to extract the contribution of axisymmetrical pairing to the sound production.

Results of the PIV measurements have shown apparent variations of the circulation, impulse, and kinetic energy of the system constituted by the two pairing vortices of about 10%. Without an analogy it would, therefore, be impossible to determine the effect of vortex pairing on the sound radiated by the flow. When the vortex sound theory, was applied, a prediction of the sound produced could be obtained. The sound production determined from the experimental data agrees with results obtained by previous authors on the basis of theoretical models, as well as the order of magnitude of the peak emission that occurs at the moment at which the two rings are coplanar. The predicted sound pulse found during the leapfrogging agrees with both the blob model of Kambe and Minota[13] and direct numerical simulations performed using experimental data as initial conditions. This demonstrates that our conservative formulation of the vortex sound theory can compensate for inaccuracies in the flow data to obtain a reliable sound prediction.

Appendix: Initial Conditions for the Numerical Simulation

The numerical code developed by Verzicco et al.[14] allows the calculation of the evolution of the vortex rings starting from an initial distribution of vorticity. The grid spacing for the direct numerical simulation (DNS) was $0.005D$ (nozzle diameters) in the radial direction and $0.015D$ in the axial direction. This is more resolved than for the PIV measurements: $0.0385D$ in both directions (ignoring the window overlap). We did not investigate the effect of the spatial resolution on the sound prediction. It was only verified that the DNS calculations were grid independent for the resolution specified.

The vortices are initially located on the same radius and are separated by a distance d. The distribution of the vorticity in the vortex cores is assumed to be Gaussian. A velocity field obtained from PIV measurements capturing a close field of view of the two vortex cores before merging has been used to characterize the initial distribution of vorticity. Figure 7 shows the vorticity field (gray levels) and the radial and axial profiles of the vorticity across the cores of the leading and trailing rings.

These vorticity profiles have been least-square fitted by a Gaussian function:

$$\omega(r) = \Gamma/\pi\sigma^2 \exp(-r^2/\sigma^2) \tag{A1}$$

to obtain the initial circulation Γ and core size σ of the rings. Because the distribution of vorticity across the cores of the vortex rings is not isotropic at this stage of their evolution, the average between the two core sizes σ and circulations Γ càlculated from the radial and axial profiles has been considered. Finally, we assume that the leading and trailing ring are identical at the instant at which they have the same radius. We then use the average of their characteristics to provide the same initial conditions of both rings. The mean values obtained are $\sigma_{\text{init}}/D = 0.088$ and $\Gamma_{\text{init}}/U_0 D = 0.55$. The initial distance d between the vortex rings cannot be obtained from the measurements because the situation in which both rings have the same radius is never met in practice. The separation d has been evaluated from the excitation parameters: Assuming that the convection speed of the vortices is approximately half the outlet velocity, we have $d = U_0/2f_e$ in which the excitation frequency f_e can be expressed by $f_e \simeq U_0/D$ for a Strouhal number of order unit. We find $d_{\text{init}} \simeq D/2$.

Acknowledgments

The authors are indebted the von Kármán Institute for Fluid Dynamics for funding the present research and to M. L. Riethmuller for fruitful discussions.

References

[1]Ffowcs Williams, J. E., "Hydrodynamic Noise," *Annual Review of Fluid Mechanics*, Vol. 1, 1969, pp. 197–222.

[2]Lighthill, M. J., "On Sound Generated Aerodynamically. Part I. General Theory," *Proceedings of the Royal Society of London*, Vol. A211, 1952, pp. 564–587.

[3]Lighthill, M. J., "On Sound Generated Aerodynamically. Part II. Turbulence as a Source of Sound," *Proceedings of the Royal Society of London*, Vol. A222, 1954, pp. 1–32.

[4]Kopiev, V. F., and Chernyshev, S. A., "Vortex Ring Eigen-Oscillations as a Source of Sound," *Journal of Fluid Mechanics*, Vol. 341, 1997, pp. 19–57.

[5]Tang, S. K., and Ko, N. W. M., "A Study on the Noise Generation Mechanism in a Circular Air Jet," *Journal of Fluids Engineering*, Vol. 115, 1993, pp. 425–435.

[6]Leung, R. C. K., Chu, W. F., Tang, S. K., and Ko, N. W. M., "Control of Vortex Pairing Sound," *AIAA Journal*, Vol. 35, No. 5, 1997, pp. 802–809.

[7]Bridges, J. E., and Hussain, A. K. M. F., "Roles of Initial Conditions and Vortex Pairing in Jet Noise," *Journal of Sound and Vibration*, Vol. 117, No. 2, 1987, pp. 289–311.

[8]Ryu, K. W., and Lee, D. J., "Sound Radiation from Elliptic Vortex Rings: Evolution and Interaction," *Journal of Sound and Vibration*, Vol. 200, No. 3, 1997, pp. 281–301.

[9]Bridges, J. E., and Hussain, A. K. M. F., "Direct Evaluation of Aeroacoustic Theory in a Jet," *Journal of Fluid Mechanics*, Vol. 240, 1992, pp. 469–501.

[10]Schram, C., and Hirschberg, A., "Application of Vortex Sound Theory to Vortex-Pairing Noise: Sensitivity to Errors in Flow Data" *Journal of Sound and Vibration*, Vol. 266, No. 5, 2003, pp. 1079–1098.

[11]Möhring, W., "On Vortex Sound at Low Mach Number," *Journal of Fluid Mechanics*, Vol. 85, 1978, pp. 85–691.

[12]Powell, A., "Theory of Vortex Sound," *Journal of the Acoustical Society of America*, Vol. 36, No. 1, 1964, pp. 177–195.

[13]Kambe, T., and Minota, T., "Sound Radiation from Vortex Systems," *Journal of Sound and Vibration*, Vol. 74, No. 1, 1981, pp. 61–72.

[14]Verzicco, R., Iafrati, A., Riccardi, G., and Fatica, M., "Analysis of the Sound Generated by the Pairing of Two Axisymmetric Co-Rotating Vortex Rings," *Journal of Sound and Vibration*, Vol. 200, No. 3, 1997, pp. 347–358.

[15]Crighton, D. G., Dowling, A. P., Ffowcs Williams, J. E., Heckl, M., and Leppington, F. G., *Modern Methods in Analytical Acoustics—Lecture Notes*, Springer-Verlag, London, 1992.

[16]Crighton, D. G., "Acoustics as a Branch of Fluid Mechanics," *Journal of Fluid Mechanics*, Vol. 106, 1981, pp. 261–298.

[17]Powell, A., "Vortex Sound: An Alternative Derivation of Möhring's Formulation," *Journal of the Acoustical Society of America*, Vol. 97, 1995, pp. 684–686.

[18]Powell, A., "Vortex Sound Theory: Direct Proof of Equivalence of 'Vortex Force' and 'Vorticity-Alone' Formulations," *Journal of the Acoustical Society of America*, Vol. 97, 1995, pp. 1534–1537.

[19]Saffman, P. G., *Vortex Dynamics*, Cambridge Monographs on Mechanics and Applied Mathematics, Cambridge Univ. Press, Cambridge, England, U. K., 1992.

[20]Lamb, H., *Hydrodynamics*, Dover, New York, 1932, Chap. 7.

[21]Kopiev, V. F., and Leontiev, E. A., "Some Remarks on Lighthill's Theory in Connection with Sound Radiation by Compact Vortices," *Soviet Physical Acoustics*, Vol. 32, No. 2, 1986, pp. 109–112.

[22]Möhring, W., "Sound Radiation by Two Elliptic Vortex Rings," *Journal of Sound and Vibration*, Vol. 140, No. 1, 1990, pp. 155–162.

[23]Leung, R. C. K., and Ko, N. W. M., "The Interaction of Perturbed Vortex Rings and Its Sound Generation," *Journal of Sound and Vibration*, Vol. 202, No. 1, 1997, pp. 1–27.

[24]Ko, N. W. M., Leung, R. C. K., and Tang, C. C. K., "The Interaction of Perturbed Vortex Rings and Its Sound Generation. Part II," *Journal of Sound and Vibration*, Vol. 228, No. 3, 1999, pp. 511–541.

[25]Dyson, F. W., "The Potential of an Anchor Ring, Part II," *Philosophical Transactions of the Royal Society of London*, Vol. A184, 1893, pp. 1041–1106.

[26]Shariff, K., Leonard, A., Zabusky, N. J., and Ferziger, J. H., "Acoustics and Dynamics of Coaxial Interacting Vortex Rings," *Fluid Dynamics Research*, Vol. 3, 1988, pp. 337–343.

[27]Tang, S. K., and Ko, N. W. M., "On Sound Generated from the Interaction of Two Inviscid Coaxial Vortex Rings Moving in the Same Direction," *Journal of Sound and Vibration*, Vol. 187, No. 2, 1995, pp. 287–310.

[28]Scarano, F., and Riethmuller, M. L., "Advances in Iterative Multigrid PIV Image Processing," *Experiments in Fluids*, Vol. 29, 2000, pp. S051–S060.

[29]Schram, C., and Riethmuller, M. L., "Measurement of Vortex Ring Characteristics During Pairing in a Forced Subsonic Air Jet," *Experiments in Fluids*, Vol. 33, 2002, pp. 879–888.

[30]Schram, C., "Aeroacoustics of Subsonic Jets: Prediction of the Sound Produced by Vortex Pairing Based on Particle Image Velocimetry," Ph.D. Dissertation, Technische Universiteit Eindhoven, Eindhoven, The Netherlands, Jan. 2003.

[31]Schram, C., Romera, G., Hirschberg, A., and Riethmuller, M. L., "Sound Produced by Vortex Pairing in a Forced Subsonic Axisymmetric Jet Using Particle Image Velocimetry and Vortex Sound Theory," ISMA2002, International Conf. on Noise and Vibration Engineering, Leuven, Belgium, Sept. 2002.

[32]Nogueira, J., Lecuona, A., and Rodriguez, P., "On the Design of Some PIV Postprocessing Filters," 7th International Conf. on Laser Anemometry Advances and Applications, Lisbon, 1997.

[33]Nelson, P. A., Halliwell, N. A., and Doak, P. E., "Fluid Dynamics of a Flow Excited Resonance. Part II: Flow Acoustic Interaction," *Journal of Sound and Vibration*, Vol. 91, 1983, pp. 375–402.

W. J. Devenport
Associate Editor